Proceedings of the ASME 2020
International Mechanical Engineering Congress and Exposition
IMECE2020
November 15-19, 2020, Portland, Oregon, USA

IMECE2020-23471

A THEORETICAL STUDY OF SENSOR-ARTERY INTERACTION IN NONINVASIVE ARTERIAL PULSE SIGNAL MEASUREMENT USING TACTILE SENSORS

Roman Carlo B. Roxas[1], Adam T. Harnish[1], Dylon N Johnson[1], Camrie M. Stewart[1], Dieu Nguyen[1], Erika Osbourne[1], Joshua A Wolbert[1], Linda Vahala[2], and Zhili Hao[1]

[1]Department of Mechanical and Aerospace Engineering, Old Dominion University, Norfolk, VA
[2]Department of Electrical and Computer Engineering, Old Dominion University, Norfolk, VA

ABSTRACT

This paper presents a theoretical study of sensor-artery interaction in arterial pulse signal measurement using a tactile sensor. A measured pulse signal is a combination of the true pulse signal in an artery, the arterial wall, its overlying tissue, and the sensor, under the influence of hold down pressure exerted on the sensor and motion artifact. The engineering essence of sensor-artery interaction is identified as elastic wave propagation in the overlying tissue and pulse signal transmission into the sensor at the skin surface, and different lumped-element models of sensor-artery interaction are utilized to examine how the involved factors affect a measured pulse signal. Achieving ideal sensor-artery conformity is the key for acquiring a measured pulse signal with minimum distortion. Hold-down pressure, sensor design, and overlying tissue collectively contribute to ideal sensor-artery conformity. Under ideal sensor-artery conformity, both the sensor and overlying tissue cause an increase in the measured stiffness of the arterial wall; damping and inertia of the sensor and overlying tissue also affects a measured pulse signal. The theoretical study shows the need to tailor the sensor design for different arteries and individual, and interpret estimated arterial indices with consideration of individual variations as well as instruments used.

Keywords: Arterial indices, arterial pulse signals, tactile sensors, overlying tissue, pulse signal transmission, lumped-element models, stiffness, damping, inertia

1. INTRODUCTION

Arterial pulse signals carry physiological and pathological information of the cardiovascular (CV) system and are noninvasively measured at the skin surface for arterial health assessment [1-4]. Two big categories of medical instruments for noninvasive arterial pulse signal measurement are applanation tonometry and photoplethysmography (PPG) sensors [1-4]. A PPG sensor is based on optical transduction, measures the blood volume change signal in an artery, and is used at the finger, earlobe, and forehead [1, 2]. A tonometer is essentially a tactile sensor, and comprises of a rigid, planar surface and a transducer, which converts the displacement of the planar surface into an electrical signal [5, 6]. A tonometer is commonly used at relatively large arteries, such as the radial artery (RA), carotid artery (CA), and femoral artery, and measures the pulsatile blood pressure signal in an artery [7].

To quantify the physiological and pathological information from a measured arterial pulse signal, the pulse waveform analysis (PWA) is conducted on it for estimating various arterial indices. As to a pulse signal measured using a PPG sensor, its second-order derivative is extensively used for estimating an arterial index indicative of arterial stiffness (or arterial elasticity), while its amplitude is not utilized [1, 2]. In contrast, as to a pulse signal measured using a tonometer, both the amplitude and the waveform are utilized for different arterial indices. For instance, the pulse waveforms of two pulse signals measured simultaneously at the carotid artery and the femoral artery are used to estimate carotid-femoral pulse wave velocity (cf-PWV), the gold standard for global arterial stiffness [3, 4]. The pulse waveform and amplitude of a measured pulsatile pressure signal at an artery and its accompanying radial motion of the arterial wall are combined to estimate local arterial elasticity and viscosity [8].

Despite being utilized in clinical studies for several decades, PPG sensors and tonometry still suffer from measurement accuracy and unreliability [7, 8]. Now, it is well recognized that the instruments used, individual variations (e.g., overlying tissue at an artery), and motion artifact influence estimated arterial indices. Moreover, Hold-down pressure exerted on an instrument in a measurement dramatically affects the amplitude and waveform of a measured pulse signal [9-11]. To date, it is widely accepted that the measured pulse signal with maximum amplitude is achieved at ideal flattening of the arterial wall, as will be explained later on, and should be used for estimation of arterial indices [9-11]. Although numerous

clinical studies have established clinical values of measured pulse signals for arterial health assessment [1-4], there are very few theoretical studies on sensor-artery interaction for examining the influence of hold-down pressure, the instrument used, and individual variations on a measured pulse signal and consequently estimated arterial indices.

Applanation tonometry was initially utilized for cuffless, continuous blood pressure monitoring. Pressman and Newgard [5] in 1963 developed early radial artery tonometry and modeled tonometry-artery interaction as a set of linear elastic springs, which included overlying tissue and adjacent tissue at an artery, in order to relate the measured pulse amplitude to blood pressure. Later on, Drzeviewchi et al. [6] in 1983 modeled the arterial wall as a continuum medium (instead of a linear spring) for relating the arterial wall deformation to blood pressure, but neglected the existence of overlying tissue and adjacent tissue at an artery. Recently, Singh et al. [11] conducted a computational study to examine how all the factors involved in tonometry-artery interaction, except motion artifact, affect the measured pulse amplitude and consequently the measured blood pressure at the radial artery. Similar to the two theoretical studies, this computational study did not examine the influence of the involved factors on the measured pulse waveform.

Based on micro/nano-fabrication technology, various tactile sensors and sensor arrays have recently been developed for arterial pulse signal measurement [12]. As compared with PPG sensors and tonometry, these tactile sensors feature low-cost, ease of operation, and great design flexibility. Different from a tonometer containing a rigid planar surface, a micro/nano-fabrication-based tactile sensor entails a soft microstructure for achieving the conformity of the sensor to an artery embedded under the skin surface so as to acquire a pulse signal with large amplitude. To date, only the measured pulse waveform has been utilized for estimation of arterial indices [12].

We previously developed a microfluidic tactile sensor with a 5×1 transducer array for pulse signal measurement and further developed a vibration model of the arterial wall for simultaneously estimating three arterial indices: elasticity, viscosity and radius of the arterial wall, from the measured pulse waveform [8]. Since the measured pulse amplitude is not used for such estimation, no calibration is needed. Similar to measured pulse signals using tonometry and PPG sensors, estimated arterial indices are influenced by all the factors involved in a pulse signal measurement. The ultimate goal of a pulse signal measurement is to acquire a measured pulse signal with minimum distortion from the true pulse signal in an artery, so as to achieve accuracy in estimated arterial indices. Our most recent study [12] examined the engineering essence of sensor-artery interaction in a pulse signal measurement. Based on the identified engineering essence, this paper is aimed to conduct a theoretical study for gaining a better understanding of how all the factors affect a measured pulse waveform and consequently estimated arterial indices.

2. RELATED THEORIES

2.1 Factors in sensor-artery interaction

As shown in Fig. 1(a), the microfluidic tactile sensor is built on a Pyrex substrate and entails a polydimethylsiloxane (PDMS) microstructure with an electrolyte-filled microchannel and five metal electrode pairs underneath. The electrolyte and the five electrode pairs form a 5×1 resistive transducer array. Fig. 1(b) depicts the working principle of pulse signal measurement using the sensor. The sensor is placed at the skin surface, and the transducer array is aligned perpendicular to the artery length for ease of use by a layperson. The pulsatile pressure signal in an artery transmits to the skin surface, deflects the PDMS microstructure, and registers as a resistance change signal by the transducer above the artery. Pertaining to pulse signal measurement, the key design parameter of the sensor is the PDMS microstructure thickness, h_s. The details about the sensor design, fabrication, and pulse signal measurement using the sensor can be found in the literature [7, 13].

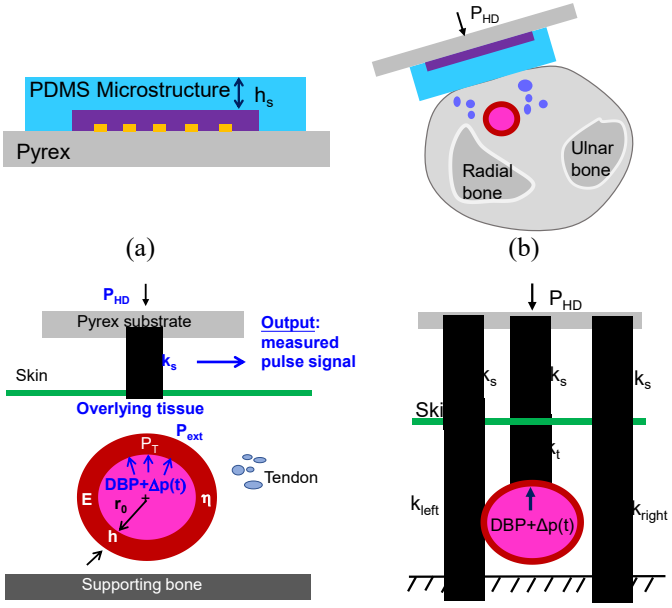

FIGURE 1: Schematics of arterial pulse signal measurement using a microfluidic tactile sensor (out of proportion for clear illustration) (a) the sensor (b) working principle for pulse signal measurement using the sensor (c) sensor-artery interaction with the factors involved being illustrated (d) Asymmetry of the adjacent tissue at an artery ($k_{left} \neq k_{right}$)

As shown in Fig. 1(c), As the input signal, the true pulse signal: pulsatile pressure, Δp(t), in an artery, is transmitted to the skin surface through overlying tissue, causes the sensor deflection at the skin surface, which is recorded by the transducer above the artery as a resistance change signal, ΔR(t). A hold-down pressure, P_{HD}, is needed for allowing the pulse signal to be transmitted into the sensor at the skin surface. Unavoidable motion artifact (i.e., respiration and body shifting of a subject and the fingers holding the sensor) causes time-

varying fluctuation of P_{HD} and time-varying displacement of the Pyrex substrate (or sensor base). As such, a measured pulse signal is a combination of the sensor, overlying tissue, the arterial wall, and the true pulse signal in an artery, under the influence of P_{HD} and motion artifact.

Adjacent tissue on the left and right sides of an artery also affects pulse signal transmission into the sensor. Asymmetry of the adjacent tissue between the left and the right side may cause uneven flattening of the arterial wall, as shown in Fig. 1(d). Similarly, any non-parallel alignment of the sensor with an artery could also cause uneven flattening of the arterial wall and lead to a measured pulse signal different from the one measured under even flattening, as shown in Fig. 2(b). Given the large size of the sensor relative to an artery, the influence of diastolic blood pressure (DBP) on a measured pulse signal might be negligible. Relative size of overlying tissue and the sensor to an artery dictates the extent to which overlying tissue and the sensor contributes to a measured pulse signal. Taken together, the factors involved in sensor-artery interaction include:

1) Sensor design (the microstructure thickness, h_s)
2) Overlying tissue
3) Hold-down pressure (P_{HD})
4) Motion artifact
5) Artery size (arterial radius, r_0, at DBP)
6) Adjacent tissue (k_{left} nd k_{right})
7) Sensor alignment

2.2 Pulse signal transmission and suppression

As shown in Fig. 2(a), the true pulse signal in an artery, as an excitation source, initiates an elastic wave propagating in overlying tissue. When there is no sensor in contact with the skin surface above an artery, the pulse signal propagating to the skin surface is reflected by the skin surface. If a sensor is simply placed at the skin surface, the pulse signal propagating to the skin surface cannot be transmitted into the sensor, due to microscopic gaps at the contact interface between the sensor and the skin surface [14]. Thus, P_{HD} on the sensor is needed to provide sensor-artery conformity so that the pulse signal can pass through the contact interface and transmit into the sensor

As illustrated in Fig. 2(b), after sensor-artery conformity is achieved, the arterial wall is partially flattened. As P_{HD} goes up, the flattened length, $L_{flatten}$, increases. According to Drzeviewchi et al. [6], there is a range of $L_{flatten}$, in which the measured pulse signal maintains its maximum amplitude, Δp_{0max}. Below the range, sensor-artery conformity is low and the measured pulse amplitude is low. Beyond the range, the true pulse signal in an artery is suppressed and the measured pulse amplitude is also low. As such, a measured pulse signal with Δp_{0max} is a tradeoff between maximizing pulse signal transmission and minimizing suppression of the true pulse signal in an artery.

2.3 Consideration of the factors in achieving ideal sensor-artery conformity $\gamma \approx 1$

Sensor-artery conformity is determined by the sensor design, surrounding tissue (overlying tissue and adjacent tissue), and P_{HD}. Here, we quantify sensor-artery conformity, γ, as follows:

i) $\gamma=0$: zero transmission,
ii) $0<\gamma<1$: partial transmission,
iii) $\gamma \approx 1$: maximum transmission with no suppression of the true pulse signal in an artery
iv) $\gamma>1$: maximum transmission with suppression of the true pulse signal in an artery.

Accordingly, $\gamma \approx 1$ represents ideal sensor-artery conformity and a measured pulse signal with Δp_{0max} is achieved at $\gamma \approx 1$. If the sensor design and surrounding tissue allow achieving $\gamma \approx 1$, then when $P_{HD}=0$, $\gamma=0$; and as P_{HD} goes up and finally leads to the pulse signal with Δp_{0max}, $\gamma \approx 1$. It is further assumed that when a measured pulse signal with Δp_{0max} is achieved, there is no suppression of the true pulse signal in an artery. Afterward, as P_{HD} continues to increase, $\gamma>1$ and the true pulse signal is suppressed. Motion artifact will cause time-varying sensor-artery conformity, $\gamma(t)$, and thus distort a measured pulse signal.

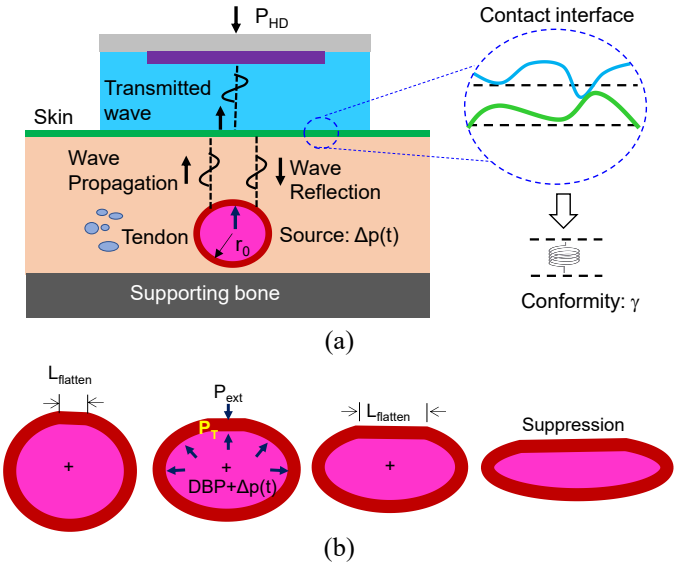

FIGURE 2: A measured pulse signal with maximum amplitude is achieved at ideal sensor-artery conformity $\gamma \approx 1$: a tradeoff between maximizing pulse signal transmission and minimizing suppression of the true pulse signal in an artery (a) elastic wave propagation and pulse signal transmission into the sensor through the contact interface (b) flattened length range for ideal sensor-artery conformity $\gamma \approx 1$

As to an artery embedded under a thick overlying tissue and surrounded by rigid tissue (e.g., tendon), a thick PDMS microstructure allows achieving $\gamma \approx 1$ and is less sensitive to motion artifact, but an extremely thick PDMS microstructure may entail a low signal-to-noise ratio. In contrast, a thin PDMS microstructure cannot deform enough upon P_{HD} to achieve $\gamma \approx 1$, and thus the measured pulse signal with Δp_{0max} is obtained at $0<\gamma<1$. As to an artery very close to the skin surface, a thin

PDMS microstructure allows achieving $\gamma \approx 1$, but can easily lead to suppression of the true pulse signal even upon a low P_{HD} and is very sensitive to motion artifact. Overall, a relatively thicker microstructure is needed for the carotid artery (CA) than for the radial artery (RA).

In this work, it is assumed that a measured pulse signal with Δp_{0max} is obtained at $\gamma \approx 1$. Under this assumption, we will examine the influence of sensor design and overlying tissue on a measured pulse signal by creating equivalent lumped-element models of sensor-artery interaction.

2.4 Equivalent lumped-element model of sensor-artery interaction

As shown in Fig. 3, the arterial wall can be treated as a lumped-element model with k, c, and m representing its spring stiffness, damping coefficient, and mass, respectively. The input signal is $\Delta p(t)$ and the output is radial motion, x_1, of the arteria wall. Similarly, the overlying tissue and the sensor can each be treated as a lumped-element model: k_s, c_s, and m_s for the sensor, and k_t, c_t, and m_t for the overlying tissue.

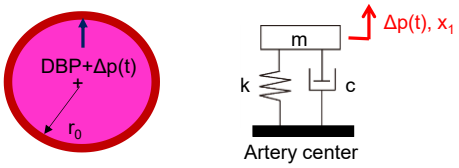

FIGURE 3: Arterial wall geometries and loads and its equivalent lumped-element model including its elastic, damping, and inertial behavior.

Fig. 4 shows how the three lumped-element models are related to each other in a pulse signal measurement. The sensor, as a 1DOF (degree-of-freedom) system, interacts with a 2DOF system (the arterial wall and the overlying tissue) to pick up the input signal, $\Delta p(t)$, at the arterial wall as the sensor deflection, x_2, which is recorded as resistance change, $\Delta R(t)$, by the sensor. Motion artifact causes base motion, $x_0(t)$, at the arterial wall and base motion, $x_3(t)$, at the sensor (Pyrex substrate). Sensor-artery conformity dictates how the sensor interacts with the 2DOF system. With $\gamma \approx 1$ being assumed, while P_{HD} may cause time-independent variation in k_s and k_t, motion artifact causes time-varying variation in γ and consequently cause time-varying variation in k_s and k_t. It is assumed that the effect of P_{HD} and motion artifact on the damping and inertial behavior of the sensor and overlying tissue is negligible in this work. As such, the factors in sensor-artery interaction are quantified as below:

1) Sensor design: k_s, c_s, and m_s
2) Overlying tissue: k_t, c_t, and m_t
3) Artery: k, c, and m
4) P_{HD} → $k_s \pm \Delta k_s$ and $k_t \pm \Delta k_t$
5) Motion artifact → $k_s(t)$ and $k_t(t)$ and $x_0(t)$ and $x_3(t)$

3. A LINEAR ELATIC MODEL

In this section, we consider solely the elastic behavior in sensor-artery interaction. Accordingly, the lumped-element model in Fig. 4 is simplified into a model consisting of three springs in series in Fig. 5. While the displacement of the arterial wall is x_1, the sensor and the overlying tissue share the same displacement, x_2. The input signal is the force coming out of the artery with a radius of r_0 at DBP: $\Delta p(t) \cdot 2r_0$. For simplicity, it is assumed that base motion, x_0, is zero. The effect of motion artifact is considered as $x_3(t)$, $k_s(t)$, and $k_t(t)$.

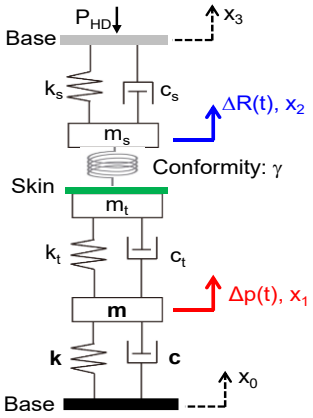

FIGURE 4: An equivalent lumped-element model of the sensor-artery interaction: the sensor, as a 1DOF system, interacts with the arterial wall and overlying tissue, as a 2DOF system, to record $\Delta p(t)$ as x_2.

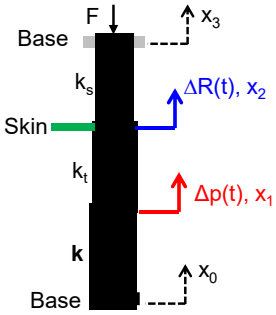

FIGURE 5: A linear elastic model of sensor-artery interaction for considering the influence of the stiffness added by the sensor and the overlying tissue

The force acting on the sensor and the force acting on the overlying tissue should be the same:

$$F = k_s(x_3 - x_2) = k_t \cdot (x_2 - x_1) \quad (1)$$

Then, the following relation holds:

$$x_1 = \frac{k_t + k_s}{k_t} \cdot x_2 - \frac{k_s}{k_t} \cdot x_3 \quad (2)$$

The force balance on the arterial wall is:

$$k \cdot x_1 = \Delta p \cdot 2r_0 + k_s \cdot (x_3 - x_2) \quad (3)$$

Substituting Eq. (2) into Eq. (3) leads to:

$$x_2 = \frac{\Delta p \cdot 2r_0 + (1 + \frac{k}{k_t}) \cdot k_s \cdot x_3}{k_s + k \cdot (1 + \frac{k_s}{k_t})} \quad (4)$$

Consequently, the displacement at the arterial wall becomes:

$$x_1 = \frac{\Delta p \cdot 2r_0 + (1 - \frac{1}{k_t / k_s + 1}) k_s \cdot x_3}{k + \frac{k_s \cdot k_t}{k_s + k_t}} \quad (5)$$

In our experimental study [12], the arterial wall, the sensor, and the overlying tissue were combined as one single DOF system with unit mass. The measured k was obtained by treating the measured x_2 as x_1 of the arterial wall. The radial artery (RA) gave rise to a higher measured k than the superficial temporal artery (STA), possibly indicating that a large artery causes a high measured k. An increase in k_s caused an increase in the measured k. Small variation in the PDMS microstructure thickness and viscoelasticity did not significantly affect the measured k. With at-rest as baseline, a significant change in the measured k with the same sensor was observed immediately post-exercise [8]. These experimental observations might imply the following relation:

$$k > k_t, \; k > k_s \quad (6)$$

In reality, k of the arterial wall is related to $\Delta p(t)$ by:

$$k \cdot x_1 = \Delta p \cdot 2r_0 \quad (7)$$

Now, we neglect motion artifact, and treat the output signal, x_2, as x_1 at the arterial wall in Eq. (5):

$$x_1 = \frac{\Delta p \cdot 2r_0}{k + \frac{k_s \cdot k_t}{k_s + k_t}} \quad (8)$$

Comparison of Eq. (7) with Eq. (8) indicates that the measured k is actually $k + \frac{k_s \cdot k_t}{k_s + k_t}$, instead of k. Thus, both k_s and k_t contribute positively to the measured k. Then, minimizing k_s will alleviate the effect of k_s on the measured result. Since a high k_t corresponds to a thicker overlying tissue, the actual k in an obese subject might be not as high as the measured k.

If motion artifact is not included and ideal sensor-artery conformity is also achieved, the linear elastic model indicates that overlying tissue and the sensor do not affect the measured pulse waveform. This is also a proof that the damping and inertial behavior of the sensor and overlying tissue is not negligible, as will be seen in Sec. 4 and 5.

Now, we relate k of the arterial wall to elasticity, E, of the arterial wall. The pure elastic constitutive model of the arterial wall states that pulsatile pressure generates the circumferential force, ΔT_θ:

$$\Delta T_\theta = E_{\theta\theta} \cdot h \cdot \frac{u_r}{r_0} = r_0 \cdot \Delta p \quad (9)$$

where $E_{\theta\theta}$ is the circumferential elasticity of the arterial wall. Combining Eq. (7) and (9) gives rise to:

$$k = 2E_{\theta\theta} \frac{h}{r_0} \quad (10)$$

A large artery has a low $E_{\theta\theta}$, and is expected to have a low measured k. Yet, the measured k at the RA is larger than that at the STA. This might indicate that overlying tissue has a non-negligible contribution to the measured k.

4. A SINGLE DEGREE-OF-FREEDOM MODEL

As shown in Fig. 6, a single degree-of-freedom (DOF) model is utilized to consider the elastic, damping, and inertial behavior of sensor-artery interaction. Note that K, C, and M represent the collective behavior of the sensor, overlying tissue, and the arterial wall. The input is pulsatile pressure, and the output is the displacement, x_1, of M. By varying the values of C and M and keeping K constant, we can examine the influence of the damping and inertia added by the sensor and overlying tissue on a measured pulse signal.

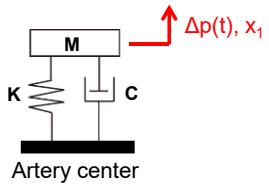

FIGURE 6: A single DOF model of sensor-artery interaction for considering the influence of the damping and inertia added by the sensor and the overlying tissue

4.1 Related values in the literature

Table 1(a) and (b) summarizes the values of K, C, and M estimated from the measured pulsatile pressure and radial motion of the arterial wall of different groups of subjects in the literature. These values were obtained by processing the pulsatile pressure signal and the radial motion signal simultaneously measured at an artery by using the related data-processing algorithms [15, 16]. Table 1(c) summarizes their values estimated from a measured pulse signal of one subject using the tactile sensor in Fig. 1 in our previous study [8]. Separately conducted by different research groups, the three studies involved different instruments on different subjects. While the study on normotensive vs hypertensive and the study on at-rest vs immediately post-exercise measured pulse signals at the carotid artery, the study on smoking vs non-smoking measured pulse signals at the index and middle fingers. The related algorithms for estimation of K, C, and M were based on physical meanings of the measured signals, rather than matching the pulsatile pressure to the radial motion. The details

about each study and estimation methodologies can be found in the related references [8, 15, 16].

Table 1 Estimated values of K, C, and M of the arterial wall from measured signals (a) at the carotid artery on two groups of subjects [15] (b) at the digital artery (i.e., fingers) on two groups of subjects [16] (c) at the carotid artery on one human subject [8]

(a)

Parameters	Normotensive (n=12)	Hypertensive (n=12)
K (a.u.)	11820	21882
C (a.u.)	962	1748
M (a.u.)	4.5	7.69

(b)

Parameters	Non-smoking	Smoking
M (a.u.)	0.028	0.055
1/K (a.u.)	0.045	0.024
C (a.u)	0.008	0.025

(c)

Parameters	At-rest	Immediately post-exercise
M (a.u.)	1	1
K (a.u.)	349.28	564.77
C (a.u)	10.87	12.40

By using a measured pulse signal at the CA of a healthy 29yr-old male subject at-rest as the pulsatile pressure [8], we examined the radial motion signal using matlab with the values of K, C, and M in Table 1. As shown in Fig. 7, since the radial motion output is quite different from the pulsatile pressure input (both are normalized for comparison), these estimated values are off from the actual values of the arterial wall, particularly in the study on smoking vs non-smoking. Thus, the actual values of K, C, and M are not available, and we will assume the values of K, C, and M and vary them until the radial motion matches the pulsatile pressure.

4.2 Effect of added damping and inertia

Given slow motion of the arterial wall, the inertia of the arterial wall is mostly ignored. Thus, we kept M=1 and kept damping ratio, as defined in Eq. (11), at ζ= 0.5.

$$\zeta = \frac{C}{2\sqrt{K \cdot M}} \tag{11}$$

With the measured pulse signals at the CA from a healthy 29yr-old male subject at-rest as the pulsatile pressure signal, the simulated radial motion was found to match the pulsatile pressure at K=100,000.

We further assume that when the measured pulse signal is at its maximum amplitude, the influence of motion artifact on the measured pulse signal is negligible. Then, if the sensor and the overlying tissue are purely elastic, the measured pulse waveform should remain the same. Therefore, we hypothesize that the damping and inertia of the sensor and the overlying tissue has a non-negligible influence on a measured pulse signal. Fig. 8 shows how the measured pulse waveform is affected by added damping and added inertia (or mass).

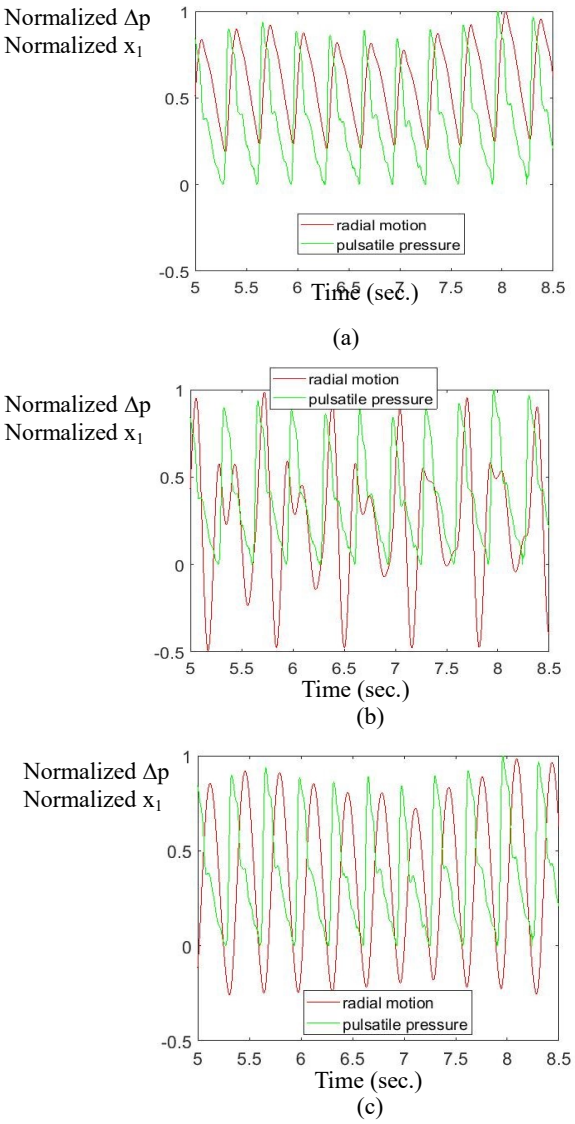

FIGURE 7: Comparison of the normalized radial motion output of the arterial wall with the normalized pulsatile pressure input using (a) the values from normotensive subjects (b) the values from non-smoking subjects (c) the values at-rest in Table 1.

Based on a vibration-model-based analysis of a pulse waveform for estimating K and C [8], we calculated K and C from the simulated pulse waveforms with added damping and inertia. Fig. 9(a) and Fig. 10(a) show how the measure K and C vary with added damping and added mass, respectively. While added damping causes a decrease in both the measured K and the measured C. In contrast, while the measured K drops with added mass, the measured C increases with added mass. Based on the relations of K and C with arterial indices [17], the influence of added damping and added mass on PWV and arterial radius, r_0, are illustrated in Fig. 9(b) and Fig. 10(b),

respectively. Both added damping and added mass entail a decrease in PWV and r_0.

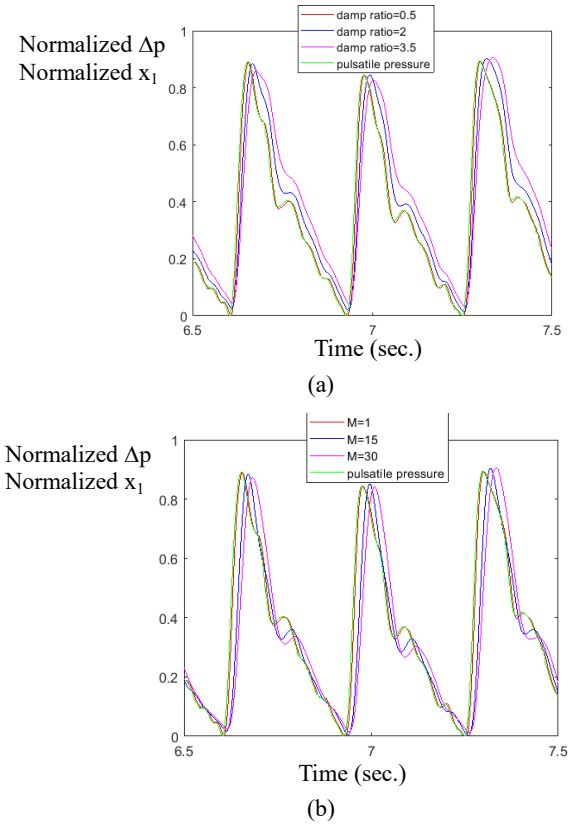

FIGURE 8: Influence of (a) added damping: ζ=0.5, ζ=2, and ζ=3.5 and (b) added mass (inertia): M=1, 15, and 30, on a measured pulse signal (K=100,000, M=1) (note that both the pulsatile pressure and the simulated radial motion at different added damping and added mass are normalized for comparison.)

5. A TWO DEGREE-OF-FREEDOM (2DOF) MODEL

As shown in Fig. 11, a 2DOF model is utilized to examine the influence of the sensor and the overlying tissue on a measured pulse signal. The corresponding state-space model is derived and is given in Eq. (12) with A, B, C, and D given in Eq. (13). Based on this state-space model, we conducted the related calculation in matlab. Fig. 12 shows how the measured pulse waveform is affected by added damping, added mass, and a combination of both. In the calculation, it is assumed that k_t=0.3k, k_s=0.1k, and c corresponds to ζ=0.5 for the arterial wall.

$$\dot{x} = B \cdot u \quad ; \quad x = \begin{bmatrix} x_1 \\ x_2 \\ \vdots \\ \vdots \end{bmatrix} \quad ; \quad y = \begin{bmatrix} \Delta p(t) \\ 0 \end{bmatrix} \qquad (12)$$
$$y = C \cdot x + D \cdot u$$

with

$$A = \begin{bmatrix} 0 & 0 & 1 & 0 \\ 0 & 0 & 0 & 1 \\ -\dfrac{k+k_s}{m} & \dfrac{k_t}{m} & -\dfrac{c+c_t}{m} & \dfrac{c_t}{m} \\ \dfrac{k_s}{m_t+m_s} & -\dfrac{k_t+k_s}{m_t+m_s} & \dfrac{c_t}{m_t+m_s} & -\dfrac{c_t+c_s}{m_t+m_s} \end{bmatrix};$$

$$B = \begin{bmatrix} 0 & 0 \\ 0 & 0 \\ \dfrac{1}{m} & 0 \\ 0 & \dfrac{1}{m_t+m_s} \end{bmatrix}; \; C = \begin{bmatrix} 1 & 0 & 0 & 0 \\ 0 & 1 & 0 & 0 \end{bmatrix}; \; D = \begin{bmatrix} 0 & 0 \\ 0 & 0 \end{bmatrix} \qquad (13)$$

Since the measured waveform is affected by added damping and added mass of the sensor and the overlying tissue, it is expected that the estimated values of arterial indices will also be affected. Fig. 13 and 14 shows the influence of added damping and added, mass, respectively, on the measured K and C and consequently estimated values of PWV and r_0. Both added damping and added mass entail decrease in the estimated values of PWV and r_0.

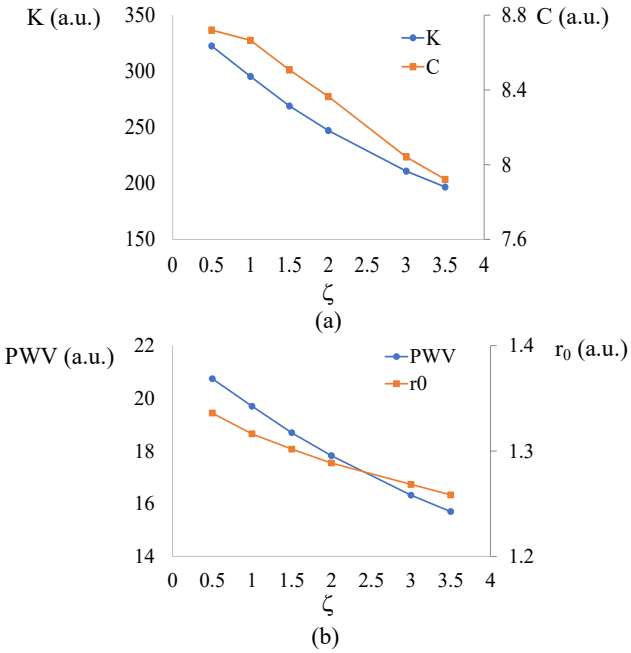

FIGURE 9: The influence added damping on (a) the measured K and C (b) estimated PWV and r_0 (K=100,000, M=1)

6. DISCUSSION

6.1 Importance of achieving ideal sensor-artery conformity

Given that the values of arterial indices are estimated from a measured pulse signal, acquiring a measured pulse signal with

minimum distortion holds the key for measurement accuracy. Quite a few factors are involved in sensor-artery interaction of a pulse signal measurement, and need to be studied for their influence on a measured pulse signal. The identified engineering essence of sensor artery interaction underscores the importance of achieving ideal sensor-artery conformity $\gamma \approx 1$ for acquiring a measured pulse signal with minimum distortion. When $0<\gamma<1$, pulse signal transmission into the sensor at the skin surface is low. When $\gamma>1$, the true signal in an artery is suppressed. Both low transmission and suppression translate to a measured pulse signal with low amplitude and high distortion. The extent of distortion increases with γ being either well above 1 or well below 1. In contrast, when $\gamma \approx 1$, pulse signal transmission into the sensor at the skin surface reaches maximum and meanwhile the true pulse signal in an artery is minimally suppressed. As such, a measured pulse signal with minimum distortion corresponds to a measured pulse signal with Δp_{0max}.

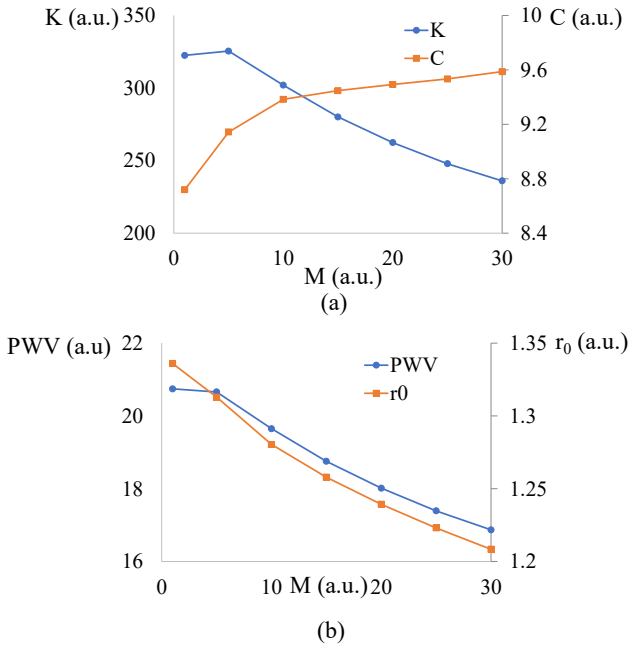

FIGURE 10: Influence of added mass on (a) the measured K and D (b) estimated PWV and r_0 (K=100,000, ζ=0.5)

In a recent experimental study on the influence of different instruments on estimated arterial indices [10], it was found that a measured pulse signal reached maximum amplitude at medium contact force (or P_{HD}), and had a low amplitude at both low and high contact force, regardless of the type of instrument used. This experimental observation validates the interpretation of sensor-artery conformity in this work. Meanwhile, a measured pulse signal with Δp_{0max} has been attributed to zero transmural pressure, P_T, in the arterial wall. The theory behind it is that when $P_T \approx 0$, the arterial wall exhibits its lowest elasticity [18]. Yet, according to this theoretical study, a measured pulse signal with Δp_{0max} results from a tradeoff between maximizing pulse signal transmission into the sensor at the skin surface and minimizing suppression of the true pulse signal in an artery.

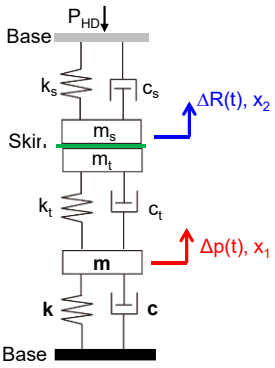

FIGURE 11: A 2DOF model for considering the influence of the sensor and the overlying tissue separately on a measured pulse signal

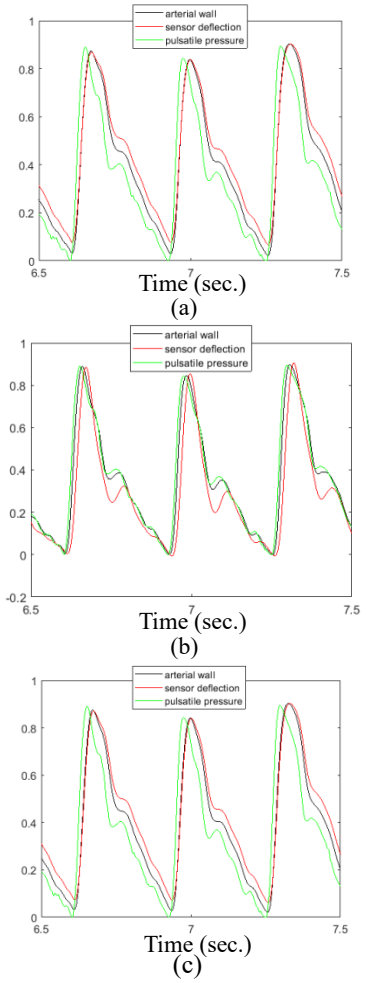

FIGURE 12: Simulated influence of (a) added damping: $c_t=c_s=10\times c$ (b) added inertia: $m_s+m_t=10$ (c) a combination of added damping and added inertia: $c_t=c_s=10\times c$ and $m_s+m_t=10$, on a measured pulse signal (k=100,000, k_t=0.3k, and k_s=0.1k, c corresponds to ζ=0.5 for the arterial wall). Note that pulse signal: normalized pulsatile pressure signal, sensor deflection: normalized x_2, and the arterial wall: normalized arterial wall deflection, x_1.

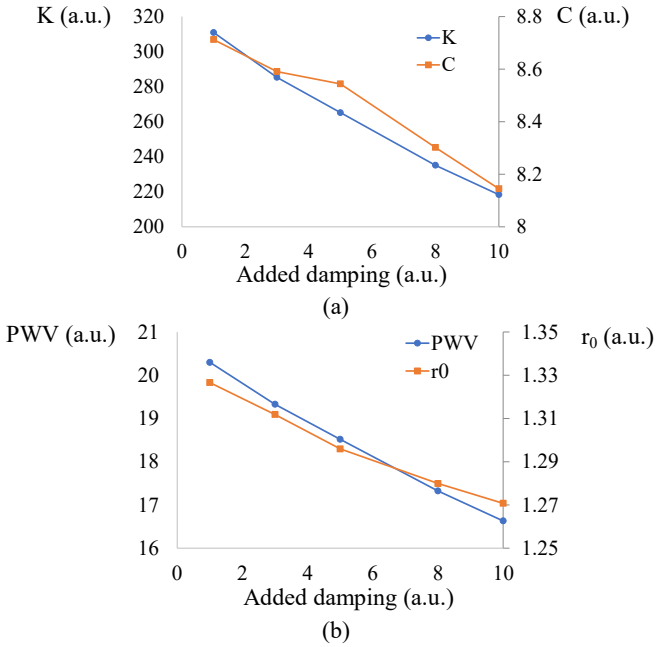

FIGURE 13: Simulated influence of (a) added damping: $c_t=c_s=c\times1$, 3, 5, 8, 10 on a measured pulse signal (k=100,000, k_t=0.3k, and k_s=0.1k, c corresponds to ζ=0.5 for the arterial wall)

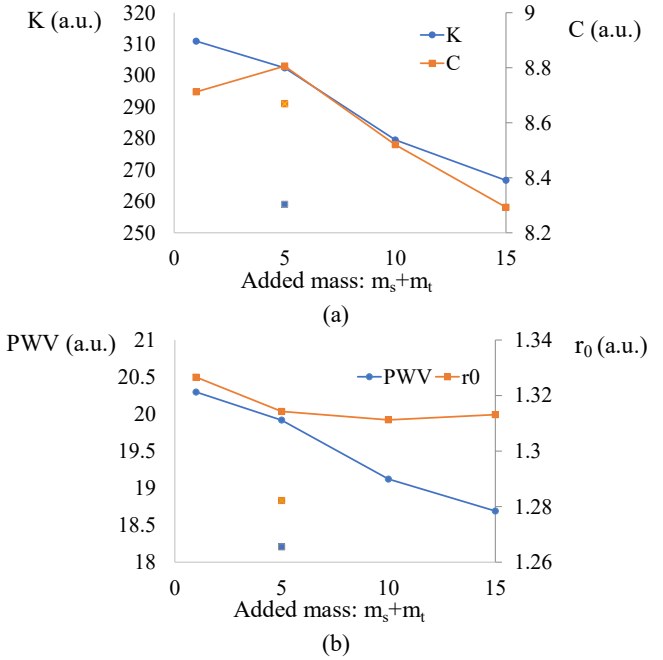

FIGURE 14: Simulated influence of added inertia: m_s+m_t=1, 5, 10, 15 on a measured pulse signal (k=100,000, k_t=0.3k, and k_s=0.1k, c corresponds to ζ=0.5 for the arterial wall)

6.2 Insights on interpretation of estimated arterial indices

Sensor design, overlying tissue, and P_{HD} collectively contribute to ideal sensor-artery conformity. Yet, overlying tissue varies between different arteries (e.g., CA versus RA) and different individuals, and thus sensor design needs to be tailored for different arteries and individuals so that ideal sensor-artery conformity can be achieved by varying P_{HD}. Then, under ideal sensor-artery conformity, a measured pulse signal is affected by sensor design and overlying tissue.

To examine the influence of sensor design and overlying tissue on a measured pulse signal, different lumped-element models are developed for illustrating different aspects of their influence. While the linear elastic model is applicable for relating the measured pulse amplitude to blood pressure, but predicts no influence of sensor design and overlying tissue on the measured pulse waveform. However, the linear elastic model provides a theoretical proof that the sensor and overlying tissue cause an increase in the measured k of the arterial wall.

Since the linear elastic model implies no influence of the sensor and overlying tissue on the measured pulse waveform, it is concluded that their damping and inertia might not be negligible. In most clinical studies, damping and inertia of the arterial wall are neglected. The single DOF model, which encompasses the sensor, overlying tissue, and the arterial wall, validates non-negligible influence of damping and inertia of the arterial wall, the sensor and the overlying tissue. The 2DOF model also validates non-negligible influence of damping and inertia of the sensor and overlying tissue. While added damping and inertia of the sensor and overlying tissue cause decrease in the measured K and C, their added stiffness entails increase in the measured K. Then, estimated arterial indices are contaminated by the stiffness, damping, and inertia of the sensor and overlying tissue. As such, interpretation of estimated arterial indices must consider anatomical structure of an artery under measurement, individual variations, and the instrument used for pulse signal measurement.

6.3 Study limitations

There are three major assumptions in this study. First, a measured pulse signal is used to represent the true pulse signal in an artery in the lumped-element models. Second, the influence of motion artifact on a measured pulse signal at $\gamma\approx1$ is assumed to be negligible. Lastly, the measured pulse signal used in the lumped-element models is assumed to be measured at $\gamma\approx1$. With these assumptions, the stiffness, damping, and inertia of the sensor and overlying tissue can be examined for their influence on estimated arterial indices.

Although the rudimentary lumped-element models in this study cannot completely capture the actual behavior in sensor-artery interaction, they still provide insights into the nature of the pulse signal measurement problems and prove the need to tailor the sensor design for different arteries and individuals, and the need to interpret estimated arterial indices with consideration of individual variations and instruments used.

7. CONCLUSION

In this work, based on the engineering essence of sensor-artery interaction in pulse signal measurement, ideal senor-artery conformity is identified as the key for acquiring a measured pulse signal with minimum distortion. With ideal sensor-artery conformity, the influence of the sensor and

overlying tissue on a measured pulse signal was examined using different lumped-element models. The stiffness, damping, and inertia of the sensor and overlying tissue all affect the values of arterial indices estimated from a measured pulse signal, underscoring the need of interpretation of estimated arterial indices with consideration of individual variations and instruments used.

ACKNOWLEDGEMENTS

This work is financially supported by NSF under Grant No. 1936005.

REFERENCES

[1] Castaneda, D., Esparza, A., Ghamari, M. Soltanpur, C., and Nazeran, H., 2018, "A Review on Wearable Photoplethysmography Sensors and Their Potential Future Applications in Health Care", International Journal of Biosensors & Bioelectronics, 4(4), pp. 195-202.

[2] Elgendi, M., Fletcher, R., Liang, Y., Howard, N. Lovell, N.H., Abbott, D. Lim, K. and Ward, R., 2019, "The Use of Photoplethysmography for Assessing Hypertension", NPJ Digital Medicine, Vol. 60.

[3] Jiang, B., Liu, B., McNeill, K., and Chowienczyk, P., 2008 "Measurement of Pulse Wave Velocity Using Pulse Wave Doppler Ultrasound: Comparison with Arterial Tonometry", Ultrasound in Medicine & Biology, 34(3), pp. 509-512.

[4] Stojadinovic, B., Nestorovic, Z., Djuric, B., Tenne, T., Zikich, D., and Žikic, D., 2017, "Laboratory Model of the Cardiovascular System for Experimental Demonstration of Pulse Wave Propagation", Physics Education, 52(2).

[5] Pressman, G., and Newgard, P., 1963"A Transducer for the Continuous External Measurement of Arterial Blood Pressure", IEEE Tansactions on Bio-Medical Engineering, Apr; 10: pp. 73-81.

[6] Drzewiecki, G.M., Melbin, J., and Noordergraaf A., 1983, "Arterial Tonometry: Review and Analysis", Journal of Biomechanics, 16(2), pp. 1441-152.

[7Wang, D., Shen, J., Mei, L., Qian, S., Li, J., and Hao, Z., 2017, "Performance Investigation of a Wearable Distributed-Deflection Sensor in Arterial Pulse Waveform Measurement," IEEE Sensors Journal, 17(13), pp. 3994-4004.

[8] Wang, D., Reynolds, L., Alberts, T., Vahala, L., and Hao, Z., 2019, "Model-based analysis of arterial pulse signals for tracking changes of arterial wall parameters: a Pilot Study," Biomechanics and Modeling in Mechanobiology, 18(6), pp. 1629-1638.

[9] He, D., Zheng, L., Liu, J., Geng, N., Dejun, G., and Xu, L., 2014, "Variation of Radial Pulse Wave Contour Influenced by Contact Pressure", *Annual International Conference of the IEEE Engineering in Medicine and Biology Society*, IEEE Engineering in Medicine and Biology Society, 2014, pp. 5635-5638.

[10] Wang, H., Wang, L. Sun, N., Yao, Y. Hao, L., Xu, L., and Greenwald, S., 2020, "Quantitative Comparison of the Performance of Piezoresistive, Piezoelectric, Acceleration, and Optical Pulse Wave Sensors", from https://www.frontiersin.org/articles/10.3389/fphys.2019.01563/full.

[11] Singh, P., Choudhury, M., Roy, S., and Prasad, A., 2017, "Computational Study to Investigate Effect of Tonometer Geometry and Patient-Specific Variability on Radial Artery Tonometry", Journal of Biomechanics, 58, pp. 105-113.

[12] Hao, Z., and Wang, D., 2020, "Arterial Pulse Signal Amplification by Adding a Uniform PDMS Layer to a Pyrex-Based Microfluidic Tactile Sensor," IEEE Sensors Journal, 20(14), pp. 2164-2172.

[13] Gu, W., Cheng, P., Ghosh, A., Liao, Y., Liao, B, Beskok, A., and Hao, Z., 2013, "Detection of distributed static and dynamic loads with electrolyte-enabled distributed transducers in a polymer-based microfluidic device," Journal of Micromechanics and Microengineering, 23(3)

[14] Valdez, M., and Dwyer-Joyce, R., 2008, "On the Interface Stiffness in Rough Contacts Using Ultrasonic Waves", Ingeniería mecánica, tecnología y desarrollo, 3(1).

[15] Armentano R., Barra J., Santana D., Pessana F., Graf S., Craiem D., Brandani L., Baglivo H., and Sanchez R.., 2006, "Smart Damping Modulation of Carotid Wall Energetics in Human Hypertension: Effects of Angiotensin-Converting Enzyme Inhibition", Hypertension, 47(3), pp.384-390.

[16] Guerrisi M., Vannucci I., and Toschi N., 2009, "Differential Response of Peripheral Arterial Compliance-Related Indices to a Vasoconstrictive Stimulus", Physiological Measurement. 30(1), pp. 81-100.

[17] Rahman, M., Sultana, N., Vahala, L., Reynolds, L, Hao, Z, "Estimation of arterial parameters from noninvasively measured arterial pulse signals: vibration-model-based analysis," IMECE2020-24551.

[18] Teng, X., and Zhang, Y., 2007, "Theoretical Study on the Effect of Sensor Contact Force on Pulse Transit Time", IEEE Transactions on Biomedical Engineering, 54(8), pp. 1490-1498.

